Critical point of tori collision in quasiperiodically forced systems

Sergey P. Kuznetsov,[1] Eireen Neumann,[2] Arkady Pikovsky,[2] and Igor R. Sataev[1]
[1]*Institute of Radio-Engineering and Electronics of RAS, Saratov Division, Zelenaya 38, Saratov, Russia*
[2]*Department of Physics, University of Potsdam, Am Neuen Palais, PF 601553, D-14415 Potsdam, Germany*
(Received 8 December 1999)

We report on a type of scaling behavior in quasiperiodically forced systems. On the parameter plane the critical point appears as a terminal point of the tori-collision bifurcation curve; its location is found numerically with high precision for two basic models, the forced supercritical circle map and the forced quadratic map. The hypothesis of universality, based on renormalization group arguments, is advanced to explain the observed scaling properties for the critical attractor and for the parameter plane arrangement in the neighborhood of the criticality.

PACS number(s): 05.45.Df, 05.10.Cc

I. INTRODUCTION

Transition to chaos via quasiperiodicity is one of the most common scenarios of the onset of temporal disorder in dynamical systems. One rather convenient way to study subtle details of such a transition is to use quasiperiodically forced systems: in these models the frequency ratio appears as an independent parameter, and can be effectively controlled both in numerics and in experiments. It has been discovered that in quasiperiodically forced systems the transition from order to chaos is typically mediated by strange nonchaotic attractors (SNAs). The term *strange* refers to the geometrical structure of the attractors, while the term *nonchaotic* indicates absence of sensitivity of the dynamics to initial conditions (all Lyapunov exponents of SNA's are nonpositive). Nevertheless, trajectories on SNAs possess high sensitivity with respect to the phase of the quasiperiodic force, and due to this property the set of trajectories appears to be a fractal object rather than a smooth torus. The SNAs were first described by Grebogi *et al.* [1] and since then have been extensively studied numerically [2–17] and experimentally [18–20]. Moreover, SNAs have been shown to be relevant in the analysis of the Schrödinger equation with a quasiperiodic potential [2,21].

Recently, the approach based on the concepts of scaling and the renormalization group (RG), which has been proved to be extremely fruitful for understanding transitions to chaos, has been applied to the problem of the onset of a SNA. Two situations have been analyzed with this approach. The first, the so called blow-out transition to the SNA, was reported in [22]. The second case relates to the terminal point of the torus-doubling bifurcation curve, the TDT point, where the regions of torus, double torus, SNA, and chaos meet together in the parameter plane [13].

In this paper we study the dynamics associated with the terminal point of the bifurcation line, where a stable torus collides with an unstable one. We call it the *TCT point* (tori-collision terminal point). At this point the bifurcation lines of smooth [23] and fractal [12] torus collisions meet together; the attractor at this point is a fractal. Our main tool is the renormalization group. In particular, it provides universal constants describing the scaling properties of phase space and parameter space associated with the TCT point.

The paper is organized as follows. In Sec. II we discuss the phenomenology of tori collision in quasiperiodically forced systems and outline the topography of the parameter plane. A method based on rational approximations to the frequency of driving allows us to find the TCT point with high accuracy. In Sec. III we formulate the renormalization group approach and study the fixed point of the RG transformation. The universal scaling properties of the dynamics, which follow from the RG analysis, are derived and confirmed numerically in Secs. IV and V.

II. TCT CRITICAL POINT IN QUASIPERIODICALLY FORCED MAPS

In this section we introduce model maps to be studied and describe the critical situation, which we call the TCT point. First, we discuss two cases of torus-torus collision, namely, the smooth and the fractal collision, and demonstrate that the corresponding bifurcation lines meet at the TCT point. Next, we describe a method to determine this point, which is based on rational approximations to the frequency of the quasiperiodic force.

A. Smooth and fractal tori collisions

As the first example we consider a quasiperiodically forced circle map

$$x_{n+1}=x_n+b-\frac{K}{2\pi}\sin[2\pi(x_n+c)] + \epsilon\sin(2\pi y_n) \pmod 1, \tag{1}$$

$$y_{n+1}=y_n+\omega \pmod 1.$$

The dynamical variable x is defined on the circle $0\leqslant x<1$. The variable y describes the phase of the external force; it also varies from 0 to 1. The parameters K and b are the usual parameters of the circle map, while the amplitude ϵ and the frequency ω characterize the forcing: rational frequencies ω correspond to periodic, and irrational to quasiperiodic driving. In this paper we fix the frequency to be equal to the inverse golden mean $\omega=(\sqrt{5}-1)/2$.

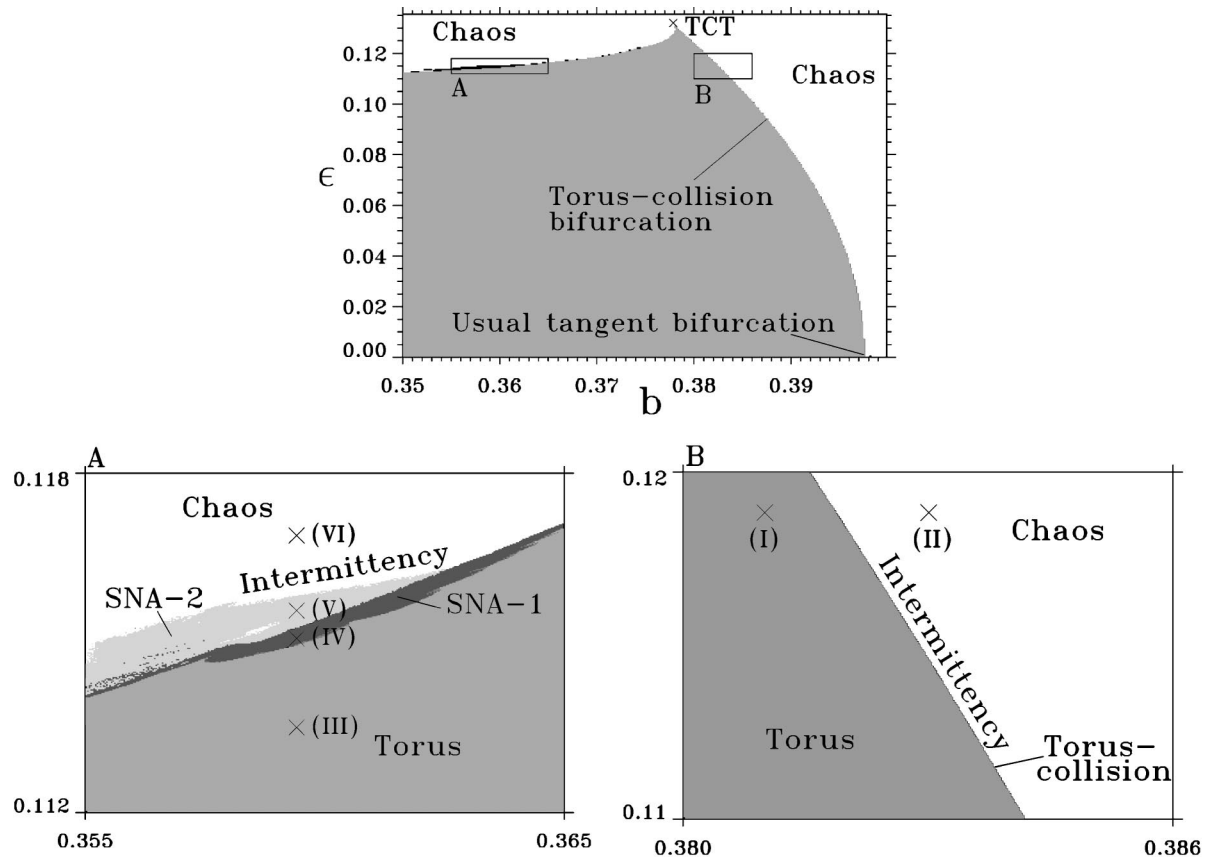

FIG. 1. The bifurcation diagram of the quasiperiodically forced circle map (1) on the (b,ϵ) plane, for fixed $k=2.5$. Regions of torus, intermittent chaos, and two types of SNA are presented. The panels A and B show the enlarged boxes of the upper panel. The phase portraits illustrating the dynamical regimes at the marked points are depicted in Fig. 2 below. In the upper panel one can observe joining of the two different boundaries of the torus area at the TCT critical point.

We intend to consider here only the supercritical circle map, $K>1$. In this case the map as a function of x is irreversible and nonmonotonic, i.e., it has maxima and minima. For a given K it is convenient to set $c=\arctan(\sqrt{K^2-1})/2\pi$ to place the minimum of the map exactly at $x=0$. We take an arbitrarily fixed value of $K=2.5$ (see the discussion below of the role of this parameter) and present the numerically obtained chart of the parameter plane (b,ϵ) in Fig. 1. The regions of different dynamical regimes are shown in gray scale. The phase plane portraits at representative points marked by crosses illustrate different dynamical regimes (Fig. 2).

To understand in more detail the arrangement of the parameter plane let us start with the vanishing amplitude of the external force $\epsilon=0$. One can easily find a value of b for which the map (1) has a stable and an unstable fixed point in the region where $dx_{n+1}/dx_n>0$; see Fig. 3. With increasing b these fixed points come closer to one another; finally, they collide (the multiplier of the fixed point becomes equal to 1) and then disappear. The moment of collision corresponds to the tangent, or saddle-node, bifurcation [24]. After that, in the region where the former fixed points were located, a narrow channel remains, which the dynamical variable x passes very slowly. In the context of the transition to chaos, the motion in the channel is a laminar phase of type-I intermittency; reinjection of the trajectories after passage through the channel corresponds to one rotation of x around the circle.

If the external force is turned on, then $\epsilon\neq 0$, and instead of a stable fixed point we obtain an attractor, represented by a smooth closed invariant curve; its size grows with the amplitude of the force. In the context of continuous-time dynamical systems, this invariant curve may be thought of as a cross section of a two-dimensional torus; it is common usage to term such an attractor a torus. Note that an unstable torus exists nearby, emerged from the unstable fixed point. With increasing b, one observes a similar transition as described above, but for the tori rather than for the fixed points. That is, the two tori, one stable and the other unstable, come close, meet, and disappear (see Fig. 3). This is the case of a smooth tori collision. At the bifurcation point the stable and unstable tori coincide and form a single semistable torus. This is the situation at the instability threshold, and the Lyapunov exponent at this moment is zero (see [23] for details). This bifurcation occurs at some bifurcation curve in the parameter plane (b,ϵ) (Fig. 1). Beyond the bifurcation an intermittent regime appears, which may be regarded as a version of type-I intermittency modified by quasiperiodic driving. In Fig. 2 this transition is illustrated by panels I and II.

If we start from the tangent bifurcation in the unforced system, and increase ϵ following the line of the smooth tori collision, we observe that the semistable torus grows in size with the forcing amplitude (Fig. 4). Finally, at $b\approx 0.38$, $\epsilon\approx 0.13$, this torus touches the line $x=0$, and this is what we call the tori-collision terminal critical point.

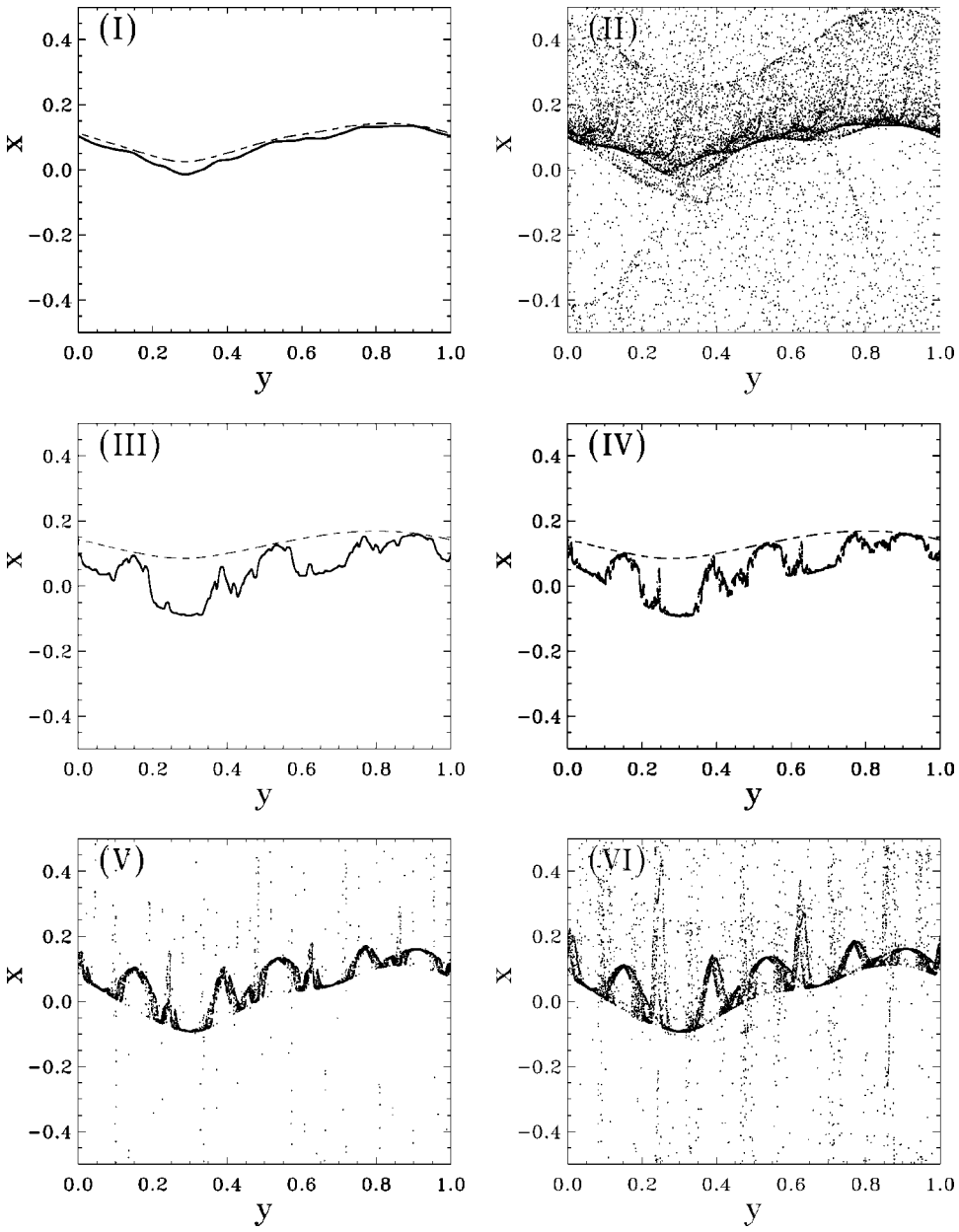

FIG. 2. Illustration of smooth and fractal tori collisions. The numbers on the panels correspond to the points marked in the bifurcation diagram Fig. 1. In I, III, and IV the stable and the unstable tori are shown with bold dots and dashed line, respectively. The transition I→II is the smooth tori collision. The transition III→IV →V→VI is a fractal tori collision. Near the collision (panel IV) the stable torus is very rumpled. The regimes V and VI differ in Lyapunov exponent; it is negative for V (thus it is a SNA) and positive for VI.

As mentioned, at the bifurcation line of the smooth tori collision the torus has zero Lyapunov exponent; the same is true at the TCT point. However, at the moment of touching the line $x=0$ one trajectory on the torus becomes superstable and has a Lyapunov exponent equal to minus infinity. Moreover, this superstable trajectory must be dense on the critical torus because of the quasiperiodic nature of the dynamics. Such a combination of properties—a threshold of instability for the invariant set as a whole, and the presence of one superstable trajectory—means that the critical torus has to be a fractal.

There is another bifurcation line of tori collision in the diagram of Fig. 1, which cannot be followed down to $\epsilon=0$. On this line the stable and unstable invariant curves touch, but do not coincide. This means that at least one of the curves must be nonsmooth, corresponding to a fractal torus. As shown in Ref. [12], such a bifurcation gives rise to a strange nonchaotic attractor. In Fig. 2 this transition is illustrated by panels III–VI.[1]

From Fig. 1 one can see that both the bifurcation lines of smooth and fractal tori collisions meet at the TCT critical point. Hence, this point is of most importance for understanding the dynamics of the system because all relevant regimes and transitions are present in the neighborhood of this point.

We argue that the properties of dynamics at the TCT point

[1]To distinguish the SNA domains we used a numerical technique based on the phase sensitivity exponent [11]. Because of the finite resolution of this technique, we cannot exclude the possibility that fractalization of the stable torus occurs, not before, but just at the moment of the tori collision. If this is the case, then the region marked as SNA-1 in Fig. 1 is occupied in fact by the regimes of smooth tori. To solve this problem, a special theoretical and numerical study is needed, which is beyond the scope of the present work.

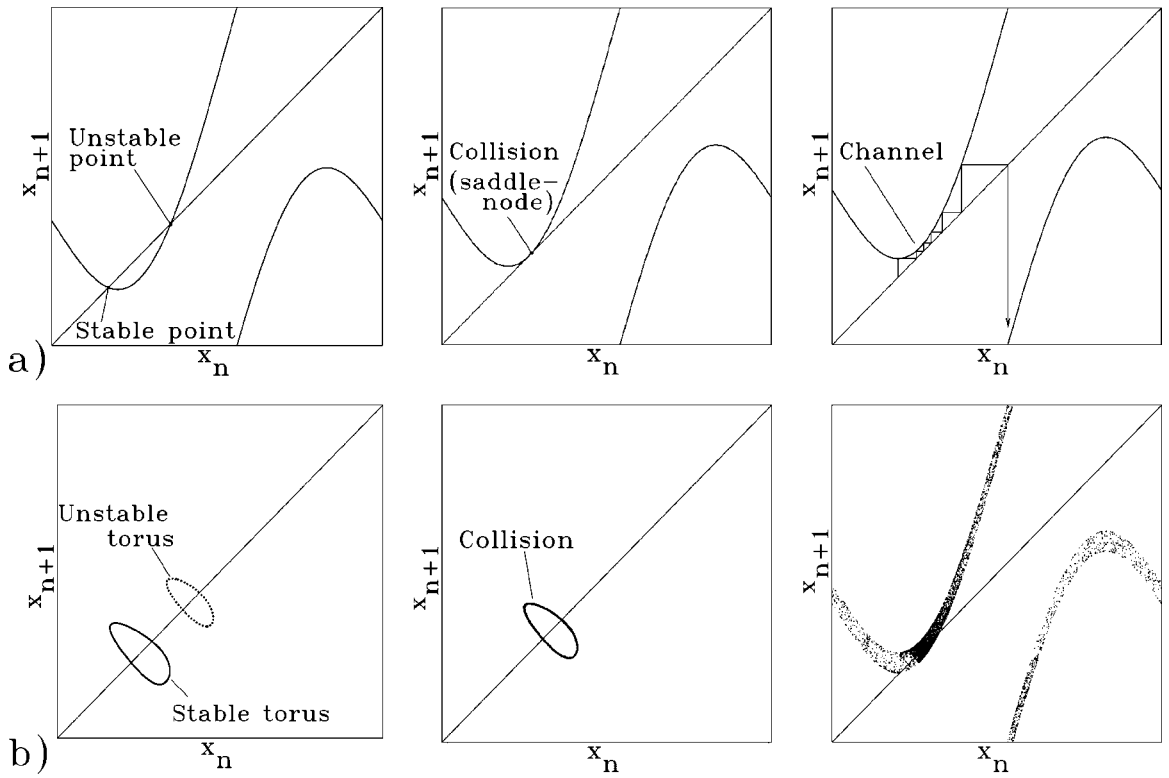

FIG. 3. Illustration of saddle-node collision. (a) The bifurcation of collision of stable and unstable fixed points in the autonomous circle map. (b) The bifurcation of tori collision in the presence of quasiperiodic forcing.

are universal. Indeed, if we go along the line of smooth tori collision, the TCT point is that where the attractor touches the singular point of zero derivative. Thus, it is essential that this singularity should be a quadratic extremum. One might expect (and this expectation will be confirmed by the renormalization group analysis below) that any one-dimensional map having a quadratic extremum and demonstrating a tangent bifurcation will exhibit at some point of the parameter space the same kind of criticality under golden-mean quasiperiodic driving. In particular, for the circle map one can try other supercritical values of the parameter K. For each $K>1$ a TCT criticality may be found at some definite b and ϵ. In other words, there exists a (presumably smooth) TCT curve in the three-dimensional parameter space (K,b,ϵ). However, the situation will be distinct if the singularity of the map is not quadratic. For example, for $K=1$ the circle map has a cubic inflection point, and the nature of critical behavior becomes different; this case will be discussed elsewhere. The situation becomes yet more unclear when the singular point disappears (for $K<1$); we plan to study this case in the future.

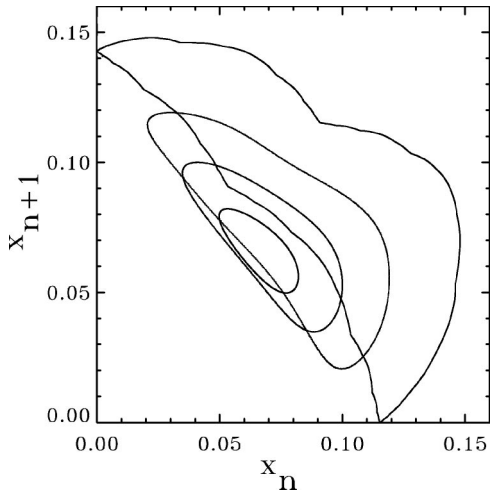

FIG. 4. The invariant curve at the smooth tori-collision point, for different values of ϵ. The smallest curve corresponds to the smallest forcing amplitude ϵ; as ϵ grows the curve becomes larger, and finally at the TCT critical point it touches the line $x=0$. This last invariant curve is fractal.

To support the argument that the existence of the TCT critical point is rather a general property of forced noninvertible maps with a quadratic extremum, we present one more example, a quadratic (logistic) map under quasiperiodic forcing:

$$x_{n+1}=x_n^2+b+\epsilon\sin(2\pi y_n),$$
$$y_{n+1}=y_n+\omega \pmod 1, \quad \omega=(\sqrt{5}-1)/2. \tag{2}$$

For vanishing amplitude of the external force $\epsilon=0$ and small b, this map possesses a stable and an unstable fixed point. At some value of $b>0$ they collide and disappear via the tangent bifurcation.

If external force is present ($\epsilon\neq 0$), we have a stable and an unstable torus that collide at some b. On increasing the amplitude of the external force and going along the bifurcation curve, we finally reach the situation where the closed invariant curve at the threshold of the torus-collision bifurcation touches the line $x=0$. This is the TCT point—the critical point of the same nature as has been described for the

TABLE I. The approximations of the TCT point for the forced circle map based on rational approximations of the driving frequency. The parameters ϵ_k, b_k converge to the TCT point; the phases u_k, v_k (initial phases for the superstable cycle and the cycle at instability threshold, respectively) converge to a definite value as well.

F_{k-1}/F_k	144/233	233/377	377/610
ϵ	0.13246827351501	0.13250795751162	0.13253613129985
b	0.37789716819380	0.37788430788852	0.37787571332547
u	0.28256543113078	0.28507911784015	0.28352121995658
v	0.28390824416939	0.28424462744230	0.28403287626312
F_{k-1}/F_k	610/987	987/1597	1597/2584
ϵ	0.13254894376094	0.13255711167252	0.13256112439438
b	0.37787164279323	0.37786912162019	0.37786785844262
u	0.28447737339461	0.28388514644255	0.28424919282601
v	0.28416035662086	0.28408010084896	0.28412859034350

circle map. As will be shown below, the critical behavior of both our models belongs to the same universality class. The disadvantage of the quadratic map in comparison to the circle map is that instead of the transition to chaos via intermittency we observe a divergence of the iterations to infinity. So the dynamics is not as rich as for the circle map; in particular, the intermittent regimes do not occur because there is no reinjection mechanism here.

B. Rational approximations to the TCT point

In order to find the critical point with high accuracy we use rational approximations to the frequency ω. In our case of the reciprocal golden mean, these approximants are the ratios of the Fibonacci numbers:

$$\omega_k = F_{k-1}/F_k, \quad k = 1,2,\ldots, \qquad F_0 = 0, \quad F_1 = F_2 = 1, \quad F_{k+1} = F_k + F_{k-1}. \tag{3}$$

If we apply a rational frequency ω_k, then, instead of the torus, we will have a cycle of period F_k. On increasing the control parameter b we expect to see a tangent bifurcation of this cycle at some parameter value that gives an approximation to the torus-collision bifurcation.

It is worth stressing here that for a rational frequency ω_k the bifurcation point depends on the initial phase y_0 of the external force. Thus, there is a whole interval of parameters between the first and the last bifurcation points. However, in the situation of smooth tori collision, this bifurcation interval tends to zero as the order of the rational approximants grows ($k \to \infty$); cf. [23]. Hence, asymptotically there is no dependence on the initial phase; this is the reason why we can speak of the smooth bifurcation of the tori. Certainly, this is the case for small amplitudes ϵ. In numerical computations, by gradually increasing the amplitude, we can trace this bifurcation up to larger amplitudes of the force.

According to our definition of the TCT point, the invariant curve corresponding to the terminal point of the torus-collision bifurcation must touch the line $x = 0$. Let us formulate the conditions for this in terms of the rational approximants. For a given rational frequency $\omega_k = F_{k-1}/F_k$ we have to find the appropriate values of $b = b_k$ and $\epsilon = \epsilon_k$ to satisfy the following conditions.

(1) For some initial phase $y_0 = u_k$ there exists a period-F_k cycle starting from $x = 0$, and the derivative dx/dy_0 vanishes. This means that the locus of periodic points for different phases of the external force—the closed curve approximating the invariant curve for irrational ω—touches the line $x = 0$.

(2) The maximal multiplier reached at some other initial phase $y_0 = v_k$ is equal to 1: for this phase the period-F_k cycle is precisely at the threshold of the tangent bifurcation. This condition means that the periodic orbit, which is stable before the bifurcation, just meets its unstable partner.

The data from our computations are summarized in Table I. Note the evident convergence of the points (ϵ_k, b_k) to a definite limit. Estimating this limit, we get the coordinates of the TCT point (ϵ_c, b_c) for the map (1). (This estimate will be essentially improved in the next section.) As a by-product, we obtain the limit values for the phases u_k and v_k: $u_c = \lim_{k\to\infty} u_k = \lim_{k\to\infty} v_k$.

It is worth explaining why we discuss the TCT point in the context of strange nonchaotic dynamics. Let us take a rational approximant ω_k and the corresponding point from Table I. Then we have simultaneously (i) a superstable cycle for one phase of the external force and (ii) a cycle at the tangent bifurcation threshold for another phase. This means that with an infinitesimal shift of the parameters b, ϵ we can face a situation where the cycle remains stable at one phase and becomes unstable at another one. Hence, changing the phase of the external force leads to a bifurcation. According to the criterion for the presence of a SNA suggested in Ref. [11], we conclude that an arbitrarily small shift of parameters from the TCT point may ensure appearance of a SNA.

Using the rational approximants for the frequency of the external force, we can find the TCT point for the logistic map (2) also. In Table II we present the corresponding numerical data. Again we observe a convergence of the points (ϵ_k, b_k) to a definite limit (ϵ_c, b_c), which is the TCT point for the quadratic map. We also obtain the limit for the phases u_k and v_k.

III. RENORMALIZATION GROUP EQUATION AND HYPOTHESIS OF UNIVERSALITY

In the case of the golden-mean frequency, which is of interest here, the main idea of the renormalization group ap-

TABLE II. The same as Table I, but for the forced quadratic map.

F_{k-1}/F_k	610/987	987/1597	1597/2584
ϵ	1.01092505020861	1.01098675212306	1.01101690728124
b	0.09981191332417	0.09979289883669	0.09978341968243
u	0.28409804003715	0.28350525381290	0.28386947751449
v	0.28378074120914	0.28370032358923	0.28374879148774
F_{k-1}/F_k	2584/4181	4181/6765	6765/10946
ϵ	1.01103504807250	1.01104434510749	1.01104972857703
b	0.09977779656842	0.09977488690490	0.09977321340337
u	0.28364394312993	0.28378268847958	0.28369681588723
v	0.28371827623344	0.28373673977169	0.28372514801896

proach is to consider a sequence of evolution operators at Fibonacci numbers of iterations [25–27,22,13]. Suppose that precisely at the critical TCT point we produce F_k iterations for one of our model maps (1) or (2) and write the result as

$$x_{n+F_k}=f_k(x_n,y_n),$$
$$y_{n+F_k}=y_n+\omega F_k \pmod 1. \tag{4}$$

In our derivation of the RG equation we will suppose that the extremum point of map f is $x=0$, and the origin for variable y is placed at the point u_c. According to the definition of the Fibonacci numbers, we can represent the evolution over $F_{k+2}=F_{k+1}+F_k$ iterations as a result of two subsequent steps, containing F_{k+1} and F_k iterations respectively. Thus, we can write [13]

$$f_{k+2}(x,y)=f_k(f_{k+1}(x,y),y+F_{k+1}\omega). \tag{5}$$

To find the new function f_{k+2} we need to use two previous functions, f_k and f_{k+1}. This may be reformulated in terms of functional pairs: To find a new pair $[f_{k+1}(x,y),\phi_{k+1}(x,y)=f_{k+2}(x,y)]$ we need one previous functional pair $[f_k(x,y),\phi_k(x,y)=f_{k+1}(x,y)]$. Indeed, from our definition and from Eq. (5) it follows that

$$f_{k+1}(x,y)=\phi_k(x,y),$$
$$\phi_{k+1}(x,y)=f_k(\phi_k(x,y),y+F_{k+1}\omega). \tag{6}$$

It is worth noting here that the second arguments of the functions f and ϕ are defined modulo 1, and due to the properties of the Fibonacci numbers, we have

$$y+F_{k+1}\omega=y-(-\omega)^{k+1} \pmod 1.$$

Now, as in any procedure in renormalization group analysis, a scale change of the variables x and y should be implemented. We set $x=X/A_k$ and $y=(-\omega)^kY$ (cf. [22,13]). After this substitution the first equation (4) transforms to

$$X_{n+F_k}=A_kf_k(X_n/A_k,Y_n(-\omega)^k),$$

and, if we wish to normalize the map in such a way that its value at the origin is 1, we have to set

$$A_k=1/f_k(0,0). \tag{7}$$

Applying the variable change to both elements of the functional pair $f_k(x,y),\phi_k(x,y)$, we introduce the rescaled functions

$$g_k(X,Y)=A_kf_k(X/A_k,Y(-\omega)^k),$$
$$G_k(X,Y)=A_k\phi_k(X/A_k,Y(-\omega)^k)=A_kf_{k+1}(X/A_k,Y(-\omega)^k). \tag{8}$$

Finally, we designate

$$\alpha_k=A_{k+1}/A_k=f_k(0,0)/f_{k+1}(0,0) \tag{9}$$

and rewrite Eqs. (6) in terms of the renormalized functions g and G to obtain the following RG equations:

$$g_{k+1}(X,Y)=\alpha_kG_k(X/\alpha_k,-\omega Y),$$
$$G_{k+1}(X,Y)=\alpha_kg_k(G_k(X/\alpha_k,-\omega Y),-\omega Y+\omega), \tag{10}$$

where

$$g_k(0,0)=1, \quad G_k(0,0)=1/\alpha_k.$$

We can calculate the terms of the functional sequence $g_k(X,Y),G_k(X,Y)$ by virtue of straightforward iterations of the original maps at the critical point. Given a Fibonacci number F_k, we first set the initial condition $x_0=0$, $y_0=u_c$ and iterate the mapping (2) F_k times. The resulting x_{F_k} is used to obtain the normalization factor $A_k=1/x_{F_k}$. Then, to find $g_k(X,Y)$ for some particular values of arguments, we again iterate the map (2), but with initial conditions $x_0=X/A_k$ and $y_0=u_c+Y(-\omega)^k$. After F_k iterations we get

$$g_k(X,Y)=A_kx_{F_k}, \tag{11}$$

and after F_{k+1} iterations

$$G_k(X,Y)=A_kx_{F_{k+1}}. \tag{12}$$

Numerical results show that at the TCT point the functions obtained for high-order Fibonacci numbers tend to a definite limit. In Fig. 5 we present an illustration for the quadratic map: For randomly chosen points (X,Y) the values of $g_k(X,Y)$ have been calculated and plotted. This has been done for several Fibonacci numbers, namely, 144, 233, and 377. One can see that the points form a well defined surface

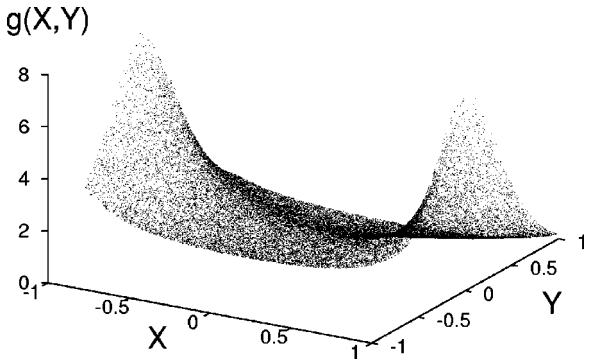

FIG. 5. The universal function: The illustration of the convergence of the functional sequence $g_k(X,Y)$ to the fixed-point solution of the RG equation. The plotted values of $g_k(X,Y)$ originate from randomly chosen points in the domain $-1<X<1$, $-\omega<Y<1$. The quadratic map was iterated for Fibonacci numbers $F_k=144,233,377$, and the scaled function was obtained by virtue of Eq. (11). Observe that the points collapse on a single surface in this three-dimensional plot.

in the space (X,Y,g). The larger the Fibonacci numbers, the higher the precision of coincidence for g_k and g_{k+1}.

This observation leads to a conjecture that there exists a fixed point of the RG equation (10) in a properly chosen space of the functional pairs. Passing to the limit $k\to\infty$ in the RG equation (10), we must have the same function in the left- and right-hand parts, so we get the fixed-point equation

$$g(X,Y)=\alpha G(X/\alpha,-\omega Y),$$
$$G(X,Y)=\alpha g(G(X/\alpha,-\omega Y),-\omega Y+\omega), \tag{13}$$

where

$$g(0,0)=1, \quad G(0,0)=1/\alpha. \tag{14}$$

Excluding the function G by means of the first equation, we can rewrite the second one as a functional equation for the single unknown function $g(X,Y)$:

$$g(X,Y)=\alpha^2 g(\alpha^{-1}g(X/\alpha,-\omega Y),\omega^2 Y+\omega). \tag{15}$$

The fixed-point equation (15) is self-consistent: it does not contain any memory of the original map. Its smooth solution, having at the origin a quadratic extremum with respect to the first argument, must be in some sense universal. The conjectured universality is supported by the fact that both our models—the quadratic map and the circle map—yield the same limit function of Fig. 5.

Being convinced of the existence of the fixed-point solution of the RG equation, we can develop a method that gives a possibility of essentially improving the accuracy of estimation of the parameter values corresponding to the TCT critical point. Let us take, for instance, the map (2). Instead of using the rational approximants we now fix $\omega=(\sqrt{5}-1)/2$. Then we try to find an appropriate set of parameters (ϵ_c,b_c,u_c), that gives coincident values of the scaling factors α_k at four subsequent levels. That is, starting iterations of Eq. (2) from $x=0,y=u_c$, we set

$$\alpha_k=\frac{x_{F_k}}{x_{F_{k+1}}}, \quad \alpha_{k+1}=\frac{x_{F_{k+1}}}{x_{F_{k+2}}}, \quad \alpha_{k+2}=\frac{x_{F_{k+2}}}{x_{F_{k+3}}},$$
$$\alpha_{k+3}=\frac{x_{F_{k+3}}}{x_{F_{k+4}}},$$

and require $\alpha_k=\alpha_{k+1}=\alpha_{k+2}=\alpha_{k+3}$. This yields three equations, from which the three unknown parameters (ϵ_c,b_c,u_c) can be found with the help of Newton's method. To construct the matrix of derivatives needed for this method, a set of mappings for derivatives x_ϵ,x_b,x_u is iterated together with the original map (2):

$$x_{\epsilon,n+1}=2x_n x_{\epsilon,n}+\sin[2\pi(y_n)],$$
$$x_{b,n+1}=2x_n x_{b,n}+1, \tag{16}$$
$$x_{u,n+1}=2x_n x_{u,n}+2\pi\epsilon\cos[2\pi(y_n)],$$

where the initial conditions are $x_{\epsilon,0}=0$, $x_{b,0}=0$, and $x_{u,0}=0$.

Using the data of the last row of Table II as an initial guess, we have implemented the above scheme step by step for subsequent levels k to obtain a more and more precise location of the critical point. For Fibonacci numbers of order 10^5 the usual double-precision arithmetic becomes insufficient, and the calculations were performed in MATHEMATICA with 60-digit precision (up to the levels $F_k=514\,229\ldots3\,524\,578$). The best result for the coordinates of the TCT critical points for the quadratic map is

$$b_c=0.099\,771\,228\,95, \quad \epsilon_c=1.011\,056\,090\,99,$$
$$u_c=0.283\,729\,413\,25 \tag{17}$$

(see Table III). Analogous computations (Table IV) performed for the circle map at $K=2.5$ with 20-digit precision up to the levels $F_k=46\,368\ldots317\,811$ yield

$$b_c=0.377\,866\,239, \quad \epsilon_c=0.132\,566\,321,$$
$$u_c=0.284\,109\,286. \tag{18}$$

All our numerical results confirm the RG conjectures, in particular, the renormalization factor α following from the calculations appears to be the same for both maps, namely,

$$\alpha\cong1.711. \tag{19}$$

However, the convergence to the universal function (see Fig. 6) is rather slow. As we have found, the convergence is governed by two components decaying as ν^k, with $\nu_1\cong0.945$ and $\nu_2\cong-0.770$.[2] This explains why we need to consider such deep levels k to be sure that the convergence to the fixed point of the RG equation indeed takes place. Also, this is the reason why the estimate (19) for α is not very precise.

[2]This observation may be used to improve the computation of the universal function $g(X,Y)$ by the iteration method.

TABLE III. The improvement of the TCT location estimate for the quadratic map, using the equalization of α at four subsequent levels. The last row gives the best estimate for the critical point.

F_k	F_{k+4}	b	ϵ	u
75025	514229	0.0997712288641926	1.0110560912888772	0.2837294133021853
121393	832040	0.0997712293313196	1.0110560897902704	0.2837294133060294
196418	1346269	0.0997712289716737	1.0110560909440631	0.2837294132590979
317811	2178309	0.0997712290364777	1.0110560907361631	0.2837294132586475
514229	3524578	0.0997712289664062	1.0110560909609621	0.2837294132482973
832040	5702887	0.0997712289735432	1.0110560909380657	0.2837294132481097
		$b_c=0.09977122895$	$\epsilon_c=1.01105609099$	$u_c=0.28372941325$

To have firm support for the hypothesis of universality, it is desirable to have a direct numerical solution of the fixed-point RG equation (15); this will provide high precision data for the universal function $g(X,Y)$ and for the factor α. One possible approach is to approximate the function by a finite polynomial containing odd and even powers of Y and even powers of X, and to search numerically for a set of coefficients of this polynomial satisfying Eq. (15) with the best possible accuracy. A straightforward realization of this idea appears not to be feasible, and we have used some tricks. First, we have selected a restricted domain of the definition for the function g in the (X,Y) plane. The condition is that for any point (X,Y) of this domain D the points $(X/\alpha, -\omega Y)$ and $(\alpha^{-1}g(X/\alpha,-\omega Y),\ \omega^2 Y+\omega)$ [see the right-hand part of Eq. (15)] belong to D. As we have the approximate data for the function g (see Fig. 5), we can check that the domain

$$D:\{-0.1+0.9y<|x|<0.1+0.9y, -\omega<y<1\} \qquad (20)$$

is appropriate. For the representation of the function in D we applied an expansion in orthogonal Chebyshev polynomials and constructed a Newtonian scheme to calculate the coefficients of this expansion. As initial guess we used the function obtained numerically from iterations of the quadratic map at the estimated TCT point. As our final result, the solution of Eq. (15) was found with precision of order 10^{-7}. The scaling constant obtained in this way is

$$\alpha=1.710\,960\,5, \qquad (21)$$

in good agreement with the previously mentioned numerical estimate (19).

IV. SCALING PROPERTIES OF THE DYNAMICS AT THE TCT POINT

In Fig. 4 one can observe that the attractor at the TCT critical point is represented by a nonsmooth fractal-like curve. We call it *the critical torus*. In this section we discuss briefly the consequences of the RG analysis for the dynamics exactly at the critical point.

Let us consider a plot of the critical attractor in the coordinates (x,y). If we rescale the variables x and $y-u_c$ by factors α and $\beta=-1/\omega$, respectively, then the dynamics is expected to remain the same (except for the rescaling of time by the factor $1/\omega$). Hence, the curve must remain invariant under this transformation. Figure 7 demonstrates that this is indeed the case: The picture inside the selected box reproduces itself under subsequent magnifications (with inversion in respect to y, due to the negative factor of the scaling). This scaling property near the origin implies that the critical curve behaves as $x\sim|y|^{\gamma}$ with the exponent $\gamma=\log\alpha/\log\beta=1.117$. The power γ is close to 1, so visually the curve looks as if it is broken at the point of singularity. In fact, $\gamma>1$, and this means that the singularity is weak: the invariant curve, apparently, remains differentiable, but not twice differentiable. Due to ergodicity ensured by irrationality of the frequency, the weak singularity at the origin implies the existence of a dense set of singularities of the same type over the whole invariant curve.

In Fig. 8(a) the Fourier spectrum is shown for the time series generated by motion on the critical attractor. It is drawn in the commonly used form, with a linear scale for the frequency and a logarithmic scale for the amplitude. This picture may be directly compared with possible experimental results. In Fig. 8(b), as in Ref. [25], we use a double loga-

TABLE IV. The same as Table III, but for the forced circle map.

F_k	F_{k+4}	b	ϵ	u
4181	28657	0.37786623026092	0.13256634957866	0.28410928832113
6765	46368	0.37786624505218	0.13256630219886	0.28410929173653
10946	75025	0.37786623782053	0.13256632536350	0.28410928671796
17711	121393	0.37786624024109	0.13256631760989	0.28410928713446
28657	196418	0.37786623890263	0.13256632189730	0.28410928614991
46368	317811	0.37786623928299	0.13256632067891	0.28410928619017
		$b_c=0.377866239$	$\epsilon_c=0.132566321$	$u_c=0.284109286$

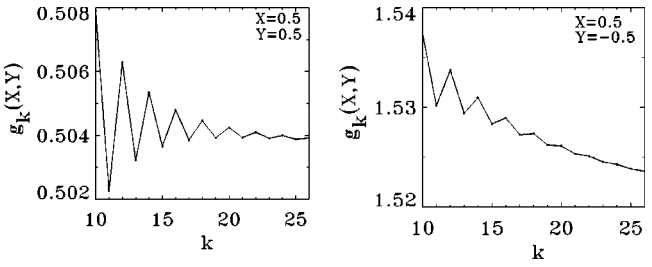

FIG. 6. The convergence of the values of $g_k(X,Y)$ for two particular pairs of the arguments (X,Y). The numerics show that for large k the convergence is dominated by a linear combination of two terms, decaying as 0.93^k and $(-0.75)^k$.

rithmic scale: it reveals the self-similar structure of the spectrum. The envelope of the family of spectral lines has a slope ≈ 3.0, in contrast to the case of the known spectrum at the golden-mean winding number in the critical circle map without external force, where the slope constant is 2. Note that for the TDT critical point [13] the slope is close to 4. In Fig. 8(c) we present the spectrum of the function $x(y)$, which describes the form of the invariant curve in Fig. 7. The powerlike decrease of the spectral amplitudes illustrates again the fractal-like nature of the critical attractor.

V. SCALING PROPERTIES OF THE PARAMETER SPACE NEAR THE TCT CRITICAL POINT

A. Linearization of the RG equation and estimation of the relevant eigenvalues

In terms of the RG approach, the investigation of a neighborhood of the TCT critical point in the parameter space is associated with small perturbations of the fixed-point solution of the functional equation (10). To simplify the analysis we use a little trick: Instead of the level-dependent factors α_k we substitute into Eq. (10) the fixed value $\alpha = \lim \alpha_k$. Certainly, the fixed point of the modified equation remains the same. Next, we set

$$\begin{aligned} g_k(X,Y) &= g(X,Y) + \nu^k h(X,Y), \\ G_k(X,Y) &= G(X,Y) + \nu^k H(X,Y), \end{aligned} \tag{22}$$

where $g(X,Y)$ and $G(X,Y)$ correspond to the fixed point and satisfy Eq. (13). The functions h and H describe a perturbation and are supposed to be small, and ν is an eigenvalue to be found. Substituting these expressions into our modified RG equation (10) and accounting for the first-order terms we obtain

$$\begin{aligned} \nu h(X,Y) &= \alpha H(X/\alpha, -\omega Y), \\ \nu H(X,Y) &= \alpha [g'(G(X/\alpha, -\omega Y), \\ &\quad -\omega Y + \omega) H(X/\alpha, -\omega Y) \\ &\quad + h(G(X/\alpha, -\omega Y)), \\ &\quad -\omega Y + \omega)], \end{aligned} \tag{23}$$

where g' denotes the derivative in the first argument. Because we have found the TCT point by tuning two free parameters, one should expect that there exist two relevant eigenvalues larger than 1, namely, $\nu = \delta_1$ and $\nu = \delta_2$, where we suppose that $\delta_1 > \delta_2$. Then, asymptotically, the behavior of an infinitesimal perturbation will contain the two corresponding eigenvectors. The coefficients at these vectors depend on the parameters of the original map and vanish at the critical point. Thus, we can write

$$\begin{aligned} g_k(X,Y) &\cong g(X,Y) + C_1(\epsilon,b)\delta_1^k h_1(X,Y) \\ &\quad + C_2(\epsilon,b)\delta_2^k h_2(X,Y), \\ G_k(X,Y) &\cong G(X,Y) + C_1(\epsilon,b)\delta_1^k H_1(X,Y) \\ &\quad + C_2(\epsilon,b)\delta_2^k H_2(X,Y). \end{aligned} \tag{24}$$

Now we can explain the procedure of calculation of the eigenvalues δ_1 and δ_2 from the iterations of the original map, e.g., quadratic map (2). Suppose we perform F_k iterations in the vicinity of the TCT critical point $\epsilon \cong \epsilon_c, b \cong b_c$, starting from $x = 0, y = u_c$. According to Eq. (24), in terms of the rescaled variable X the result will be

$$X_{F_k} \cong g(0,0) + C_1(\epsilon,b)\delta_1^k h_1(0,0) + C_2(\epsilon,b)\delta_2^k h_2(0,0). \tag{25}$$

Thus, at subsequent Fibonacci numbers of the iterations, the original variable x will behave as

$$x_{F_k} \cong \alpha^{-k}[d_0 + d_1(\epsilon,b)\delta_1^k + d_2(\epsilon,b)\delta_2^k], \tag{26}$$

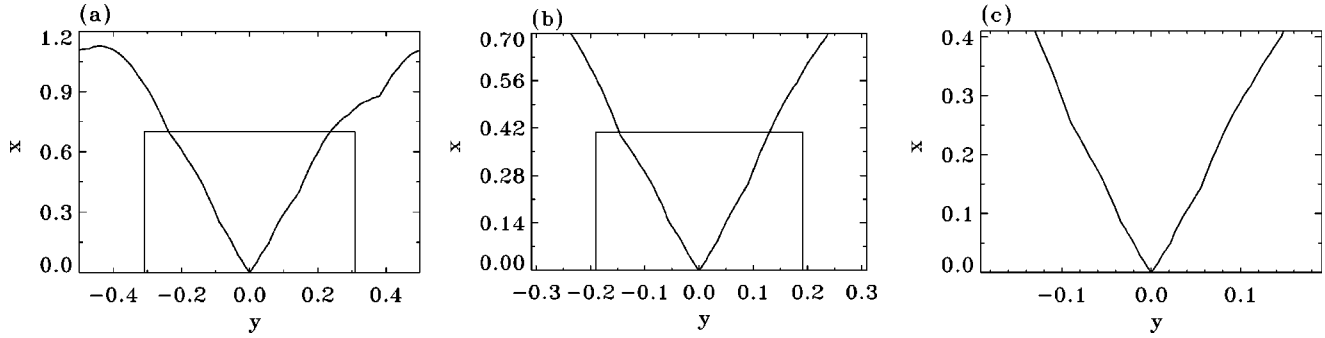

FIG. 7. The scaling of the critical torus of the quadratic map on the phase plane (x,y). Panel (a) shows the whole picture, panel (b) presents the enlargement of the box from panel (a), and panel (c) shows the enlargement of the box from panel (b). The magnification factors are $\alpha = 1.711$ for the vertical axis and $-\omega^{-1} = -1.618$ for the horizontal axis.

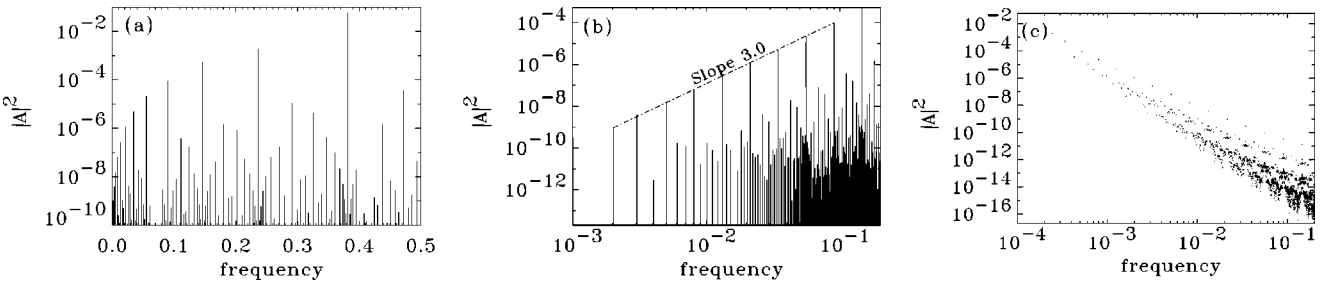

FIG. 8. The Fourier spectrum $|A(\omega)|^2$ of the time series x_n generated by the quadratic map at the TCT critical point: (a) linear scale for the frequency and logarithmic scale for the amplitude; (b) double logarithmic scale; (c) the Fourier spectrum of the periodic function $x(y)$ describing the critical torus.

where d_0, d_1, and d_2 are some combinations of the coefficients and constants. As we mentioned in the previous section, it is possible to compute the derivatives of the variable x with respect to the parameters by simultaneous iterations of the original map (2) together with Eqs. (16) at the critical point. According to Eq. (26), the derivatives will behave as

$$x_{\epsilon,F_k} \cong d_{1,\epsilon}(\epsilon_c,b_c)(\delta_1/\alpha)^k + d_{2,\epsilon}(\epsilon_c,b_c)(\delta_2/\alpha)^k,$$
$$x_{b,F_k} \cong d_{1,b}(\epsilon_c,b_c)(\delta_1/\alpha)^k + d_{2,b}(\epsilon_c,b_c)(\delta_2/\alpha)^k. \tag{27}$$

No matter which of these expressions we take, for large k the first term will dominate, and the value of δ_1 may be found from the ratio of subsequent terms,

$$\delta_1 \cong \alpha \frac{x_{\epsilon,F_k}}{x_{\epsilon,F_{k-1}}} \cong \alpha \frac{x_{b,F_k}}{x_{b,F_{k-1}}}. \tag{28}$$

To obtain δ_2, we have to select properly the direction of the perturbation in the parameter plane (ϵ,b) to exclude a contribution from the largest eigenvector. For this, we first calculate x_{ϵ,F_N} and x_{b,F_N} for the maximal Fibonacci number F_N we can handle, and require $x_{\epsilon,F_N}\Delta\epsilon + x_{b,F_N}\Delta b = 0$. For F_k smaller than F_N the derivatives with respect to a value of the shift in the direction $(\Delta\epsilon,\Delta b)$ should behave as $x_{p,F_k} \propto (\delta_2/\alpha)^k$, and δ_2 can be estimated from the ratio of the terms for subsequent k. In practice, however, a technical difficulty arises here: the derivatives appear to be in a more complicated dependence on k because of the notable contribution from the third eigenvalue, associated with a shift of initial phase from the point u_c. This is the trivial eigenvalue $\delta_3 = -(\sqrt{5}+1)/2$, and it may be excluded by using a modified ratio, namely,

$$\delta_2 \cong \alpha \frac{x_{p,F_{k+1}} - (\delta_3/\alpha)x_{p,F_k}}{x_{p,F_k} - (\delta_3/\alpha)x_{p,F_{k-1}}}. \tag{29}$$

The calculations have been performed for the quadratic map and for the circle map. For both maps the results are in good agreement, yielding

$$\delta_1 \cong 3.65, \quad \delta_2 \cong 1.81. \tag{30}$$

To compute the constants δ_1 and δ_2 with higher accuracy, one can turn to a numerical solution of the eigenproblem (23). We used the Chebyshev polynomial expansion for the universal function g (see Sec. III), the corresponding representation for G [according to Eq. (13), $G(X,Y) = \alpha^{-1} g(\alpha X, -Y/\omega)$], and analogous expansions for the functions $h(X,Y)$ and $H(X,Y)$. The relevant eigenvalues are found to be

$$\delta_1 = 3.600\,810\ldots, \quad \delta_2 = 1.828\,329\ldots, \tag{31}$$

in reasonable agreement with the estimates (30).

B. Self-similarity on the plane of parameters

From the relation for the evolution operator (24) one can see that the parameter plane near the critical point possesses some properties of self-similarity, or scaling. Indeed, suppose we consider a dynamical regime at the point (ϵ,b), which corresponds to some values of the coefficients $C_1 = C_1^0$ and $C_2 = C_2^0$. If we find a point (ϵ',b') such that the coefficients are equal to $C_1 = C_1^0/\delta_1$ and $C_2 = C_2^0/\delta_2$, then the evolution operator corresponding to F_{k+1} iterations at the new point will coincide with the evolution operator for F_k iterations at the old point. Hence, the type of dynamics (torus, chaos, SNA) should be the same at both points and differ only by the characteristic time scale: It is larger at the second point by a factor F_{k+1}/F_k, which tends to ω^{-1} as $k \to \infty$. According to this, all quantitative characteristics of both regimes can easily be expressed one via the other. For example, the Lyapunov exponents are connected as

$$\Lambda(\epsilon',b') \cong \omega\Lambda(\epsilon,b). \tag{32}$$

It is worth stressing that all the scaling relations are asymptotic, i.e., they are more precise when we are closer to the critical point.

To demonstrate the scaling numerically, it would be convenient to define an appropriate local coordinate system (*scaling coordinates*) near the critical point in such a way that the scaling transformation described above would correspond simply to the simultaneous scale change along the coordinate axes by factors δ_1 and δ_2, respectively. Unfortunately, we do not know explicit expressions for C_1, C_2 via ϵ and b, so the problem has to be resolved numerically. Let us place the origin of the desirable coordinate system (c_1,c_2) at the critical point and note, first, that one coordinate axis, corresponding to the larger scaling factor δ_1, may be directed almost arbitrarily. A shift along this direction has to contribute to the coefficient C_1 in Eq. (24); therefore, the only condition is that it must be transverse to a curve on the parameter plane given by the equation $C_1(\epsilon,b) = 0$. In contrast to

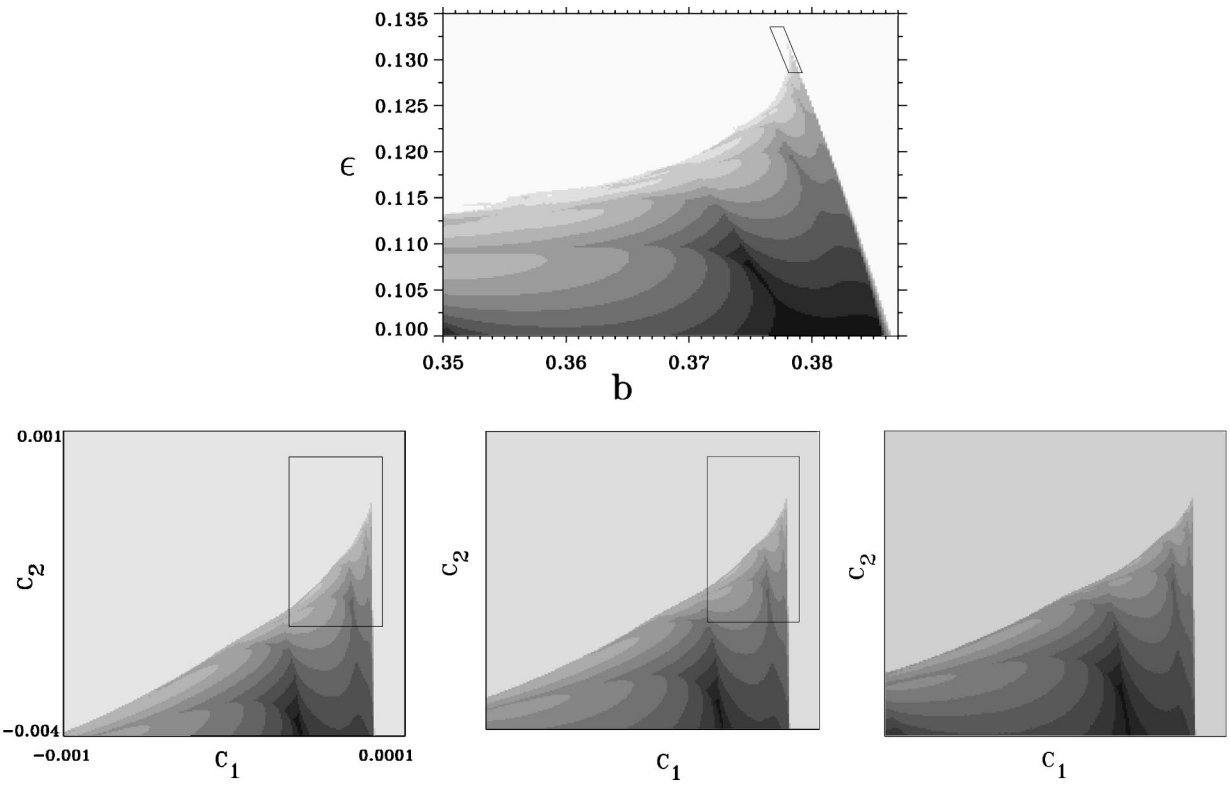

FIG. 9. A demonstration of the scaling properties on the plane of the parameters near the TCT critical point. We plot the Lyapunov exponent for the circle map using a gray scale. For clarity of presentation, only the region of negative exponents is resolved. The upper panel shows the Lyapunov exponents in the original b,ϵ coordinates. The left lower panel shows the transformation to the scale coordinates (34), and the middle and the right lower panels show successive magnifications: for each subsequent picture the horizontal scale is scaled by the factor $\delta_1=3.65$, and the vertical scale is scaled by the factor $\delta_2=1.81$. The magnitudes of the Lyapunov exponent are coded by the gray scale, from light (positive values) to dark (negative values). The coding rule from picture to picture is redefined according to Eq. (32).

this, the second coordinate must be defined carefully, because the contribution to the first eigenvector should vanish along the coordinate axis. Thus, the line defined by the equation $C_1(\epsilon,b)=0$ has to be a coordinate curve along which the value of c_2 is varied, and on which $c_1=0$. One may try to search for an explicit expression of this coordinate curve via Taylor expansion in the form

$$\Delta\epsilon=c_2, \quad \Delta b=Ac_2+Bc_2^2+Cc_2^3+\cdots. \tag{33}$$

This expansion may be cut if we take into account the concrete relation between the scaling factors δ_1,δ_2. Suppose that we consider a sequence of pictures of the parameter plane near the critical point on smaller and smaller scales, namely, $c_1\propto\delta_1^{-k}$ and $c_2\propto\delta_2^{-k}$. If we neglect the Taylor coefficient of c_2^m in Eq. (33), the deflection from the proper coordinate curve will behave as δ_2^{-mk}, and the contribution to the first eigenvector in the evolution operator (24) will be of order $\delta_2^{-mk}\delta_1^k$. This contribution is thus not dangerous if $|\delta_1|<|\delta_2^m|$. According to our estimate (31), $\delta_2<\delta_1$ and $\delta_2^2<\delta_1$, but $\delta_2^m>\delta_1$ for $m\geqslant 3$. Hence, it is sufficient to account in Eq. (33) for only the linear and quadratic terms (see [28,29] for other examples of selecting the scaling coordinates).

In the spirit of the above discussion, we define the scaling coordinates near the TCT critical point by the following ansatz, appropriate for both our model maps:

$$\epsilon=\epsilon_c+c_2, \quad b=b_c+c_1+Ac_2+Bc_2^2. \tag{34}$$

The coefficient A was defined from the ratio of derivatives at the critical point; cf. Eq. (27). The coefficient B may be obtained in the same manner from more elaborate computations involving the second derivatives. From our calculations it was found that for the quadratic map

$$A=-0.311\,707\,6, \quad B=-0.2819, \tag{35}$$

and for the circle map

$$A=-0.312\,184\,8, \quad B=-2.047. \tag{36}$$

Apparently, the coordinate curve $c_1=0$ coincides with the bifurcation curve of smooth tori collision. So the coefficient A is related to the slope of the bifurcation curve at the TCT point in the original coordinates (ϵ,b), while B is related to its curvature.

In Figs. 9 and 10 we demonstrate the scaling of the parameter plane near the TCT critical point. As indicator of the dynamical regimes the Lyapunov exponent is used. In the original parameter plane (ϵ,b) we select a small fragment near the TCT critical point with the borders going along the coordinate lines of the scaling coordinate system. The next plots show details of this fragment under subsequent magnification by factors δ_1 and δ_2 along the respective axes of the scaling coordinates. For each next diagram we change the

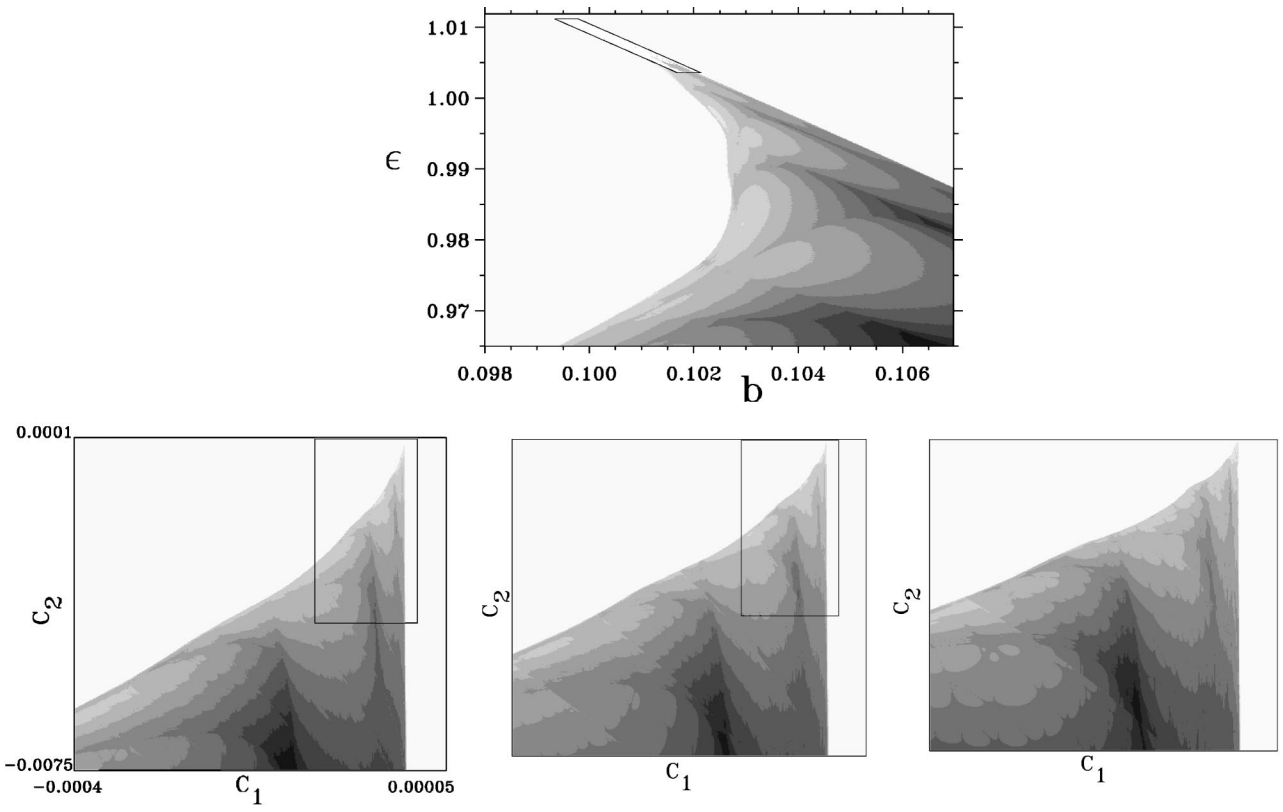

FIG. 10. The same as Fig. 9, but for the forced quadratic map.

rule of the gray scale coding in accordance with the rule of renormalization for the Lyapunov exponent (32). A nice coincidence of the plots observed at subsequent stages of magnification proves the scaling.

VI. CONCLUSION

In this paper we have reported on a type of critical behavior at the border between regular and complex dynamics. This critical behavior is associated with a point in the parameter plane of quasiperiodically forced systems, where the torus-collision bifurcation line terminates; we call it the TCT critical point. In particular, we have found a critical point of such type in the quasiperiodically forced supercritical circle map and quadratic map.

The dynamics of the circle map near this point includes all relevant regimes: torus, chaos, and strange nonchaotic attractor. Two different types of transition to chaos meet here, one from a torus to intermittent chaos via a smooth tori collision, and another from torus via fractal tori collision to SNA and chaos. For the quadratic map the ''zoo'' of regimes is not so rich, because the intermittent and chaotic regimes do not exist due to escape of trajectories to infinity. However, from the point of view of the dynamics at the critical point, this map belongs to the same universality class.

We have found the precise location of the TCT critical point for both model maps. To investigate the dynamics at the critical point we have adopted the RG approach appropriate for the golden-mean frequency of the external force; it is similar to that developed earlier for the torus-doubling terminal point [13]. We have demonstrated that properly renormalized functions describing the evolution operators over the Fibonacci numbers of iterations converge to a fixed-point solution of the RG equation, while for the TDT point it was a period-3 cycle. As follows from the RG analysis, the attractor at the TCT point (the critical torus) is represented by a fractal-like closed invariant curve, having weak singularities at a dense set of points.

The formulation of the linearized RG equation for the perturbations of the fixed-point evolution operator allowed us to derive the scaling properties of the vicinity of the critical point in the parameter plane. These scaling properties were checked in computer simulations, demonstrating good agreement with the RG results.

It may be conjectured that the universality class associated with the TCT critical point will contain not only one-dimensional maps, but also higher-dimensional systems. It would be of interest to observe this type of universal behavior in experiments similar to that performed for the observation of the TDT critical behavior [20]. However, at the moment it is not yet clear how the present analysis can be generalized to invertible maps. Indeed, in our procedure of determining the critical behavior the presence of the quadratic extremum plays a crucial role. However, it does not exist, e.g., for the forced subcritical ($K<1$) circle map, where smooth and fractal tori collisions can also be observed. This problem will be the subject of future research.

ACKNOWLEDGMENTS

We thank U. Feudel and J. Stark for discussions, and especially P. Glendinning, whose remark on the possibility of universal behavior for the forced critical circle map stimu-

lated our study. The authors acknowledge support from Max-Planck-Institut für Physik komplexer Systeme (Dresden), where a part of this work was done during the workshop ''Beyond Quasiperiodicity: Complex Structures and Dynamics.'' S.K. acknowledges support from the Deutsche Forschungsgemeinschaft (SFB 555 ''Complex Nonlinear Processes''). S.K. and I.S. acknowledge support from the RFBR (Grant Nos. 97-02-16414 and 00-02-17509).

[1] C. Grebogi, E. Ott, S. Pelikan, and J.A. Yorke, Physica D **13**, 261 (1984).
[2] A. Bondeson, E. Ott, and T.M. Antonsen, Phys. Rev. Lett. **55**, 2103 (1985).
[3] F.J. Romeiras *et al.*, Physica D **26**, 277 (1987).
[4] F.J. Romeiras and E. Ott, Phys. Rev. A **35**, 4404 (1987).
[5] M. Ding, C. Grebogi, and E. Ott, Phys. Rev. A **39**, 2593 (1989).
[6] M. Ding, C. Grebogi, and E. Ott, Phys. Lett. A **137**, 167 (1989).
[7] T. Kapitaniak, E. Ponce, and J. Wojewoda, J. Phys. A **23**, L383 (1990).
[8] J.F. Heagy and S.M. Hammel, Physica D **70**, 140 (1994).
[9] A. Pikovsky and U. Feudel, J. Phys. A **27**, 5209 (1994).
[10] M. Ding and J. Scott Kelso, Int. J. Bifurcation Chaos Appl. Sci. Eng. **4**, 553 (1994).
[11] A. Pikovsky and U. Feudel, Chaos **5**, 253 (1995).
[12] U. Feudel, J. Kurths, and A. Pikovsky, Physica D **88**, 176 (1995).
[13] S. Kuznetsov, U. Feudel, and A. Pikovsky, Phys. Rev. E **57**, 1585 (1998).
[14] Y.-C. Lai, Phys. Rev. E **53**, 57 (1996).
[15] T. Nishikawa and K. Kaneko, Phys. Rev. E **54**, 6114 (1996).
[16] T. Yalcinkaya and Y.-C. Lai, Phys. Rev. Lett. **77**, 5039 (1996).
[17] A. Witt, U. Feudel, and A. Pikovsky, Physica D **109**, 180 (1997).
[18] W.L. Ditto *et al.*, Phys. Rev. Lett. **65**, 533 (1990).
[19] T. Zhou, F. Moss, and A. Bulsara, Phys. Rev. A **45**, 5394 (1992).
[20] B. Bezruchko, S. Kuznetsov, and Ye. Seleznev (unpublished).
[21] J.A. Ketoja and I.I. Satija, Physica D **109**, 70 (1997).
[22] S. Kuznetsov, A. Pikovsky, and U. Feudel, Phys. Rev. E **51**, R1629 (1995).
[23] P.R. Chastell, P.A. Glendinning, and J. Stark, Phys. Lett. A **200**, 17 (1995).
[24] J. Guckenheimer and P. Holmes, *Nonlinear Oscillations, Dynamical Systems, and Bifurcations of Vector Fields* (Springer, New York, 1986).
[25] S.J. Shenker, Physica D **5**, 405 (1982).
[26] M.J. Feigenbaum, L.P. Kadanoff, and S.J. Shenker, Physica D **5**, 370 (1982).
[27] D. Rand, S. Ostlund, J. Sethna, and E.D. Siggia, Physica D **8**, 303 (1983).
[28] A.P. Kuznetsov, S.P. Kuznetsov, and I.R. Sataev, Phys. Lett. A **189**, 367 (1994).
[29] A.P. Kuznetsov, S.P. Kuznetsov, and I.R. Sataev, Physica D **109**, 91 (1997).